Coordination of DNA Ends During Double-Strand-Break Repair in Bacteriophage T4

Bradley A. Stohr and Kenneth N. Kreuzer[1]

Departments of Microbiology and Biochemistry, Duke University Medical Center, Durham, North Carolina 27710

Manuscript received May 4, 2002
Accepted for publication August 7, 2002

ABSTRACT

The extensive chromosome replication (ECR) model of double-strand-break repair (DSBR) proposes that each end of a double-strand break (DSB) is repaired independently by initiating extensive semiconservative DNA replication after strand invasion into homologous template DNA. In contrast, several other DSBR models propose that the two ends of a break are repaired in a coordinated manner using a single repair template with only limited DNA synthesis. We have developed plasmid and chromosomal recombinational repair assays to assess coordination of the broken ends during DSBR in bacteriophage T4. Results from the plasmid assay demonstrate that the two ends of a DSB can be repaired independently using homologous regions on two different plasmids and that extensive replication is triggered in the process. These findings are consistent with the ECR model of DSBR. However, results from the chromosomal assay imply that the two ends of a DSB utilize the same homologous repair template even when many potential templates are present, suggesting coordination of the broken ends during chromosomal repair. This result is consistent with several coordinated models of DSBR, including a modified version of the ECR model.

THREE basic models have been proposed for double-strand-break repair (DSBR) during bacteriophage T4 infection: the Szostak *et al.* (1983) model (Belfort 1990; Mueller *et al.* 1996a), the synthesis-dependent strand annealing (SDSA) model (Nassif *et al.* 1994; Mueller *et al.* 1996a), and the extensive chromosome replication (ECR) model (George and Kreuzer 1996; George *et al.* 2001). Evidence for the Szostak *et al.* and SDSA models has come from analysis of *td* intron movement between phage and plasmid substrates (Belfort 1990; Mueller *et al.* 1996a), while evidence for the ECR model has come from experiments involving repair of plasmid double-strand breaks (DSBs; George and Kreuzer 1996; George *et al.* 2001).

The Szostak *et al.* (1983) model begins with processing of the broken DNA ends to expose 3′ single-strand overhangs (Figure 1A). One of these ends invades the homologous duplex DNA and primes DNA synthesis in one direction. The second broken end anneals to the displaced template strand and primes synthesis in the opposite direction. Ligation results in a double Holliday junction structure that is subsequently resolved to complete the repair process. Synthesis-dependent strand annealing (SDSA) also begins when one processed end invades the homologous duplex DNA and initiates synthesis (Figure 1B). In this case, however, the newly synthesized strand is extruded behind a replication bubble. When the appropriate complementary region is extruded, the opposite broken end anneals to the extruded strand and initiates retrograde DNA synthesis. The repair is completed by ligation and resolution of the cross-strand structure (for review, see Paques and Haber 1999).

Both the Szostak *et al.* and the SDSA models propose that the two ends of the DSB are repaired in a coordinated manner, with both ends participating in a single repair event on the same homologous repair template. In contrast, the ECR model proposes that the two broken ends can diffuse from each other and invade different homologous templates (Figure 1C; George and Kreuzer 1996). Each invading end initiates semiconservative DNA replication, which proceeds to the end of the molecule, and Holliday junction resolution completes the repair process. Thus, each broken end is repaired independently and ultimately generates a complete repair product.

The ECR model is based upon the T4 recombination-dependent replication (RDR) mechanism (reviewed in Mosig 1983; Kreuzer 2000). While DNA replication early in T4 infection occurs in an origin-directed process, DNA replication at late times of infection depends on homologous recombination proteins and initiates throughout the genome. The RDR mechanism begins with a (randomly located) chromosomal end invading homologous genomic sequence. The invading 3′ end serves as a primer for leading-strand synthesis, and loading of the helicase/primase complex on the displaced strand ensures efficient lagging-strand synthesis. Thus, ECR is essentially a modified form of T4 RDR in which the invading DNA molecule is one end of a DSB rather

[1]*Corresponding author:* Box 3020, Duke University Medical Center, Durham, NC 27710. E-mail: kenneth.kreuzer@duke.edu

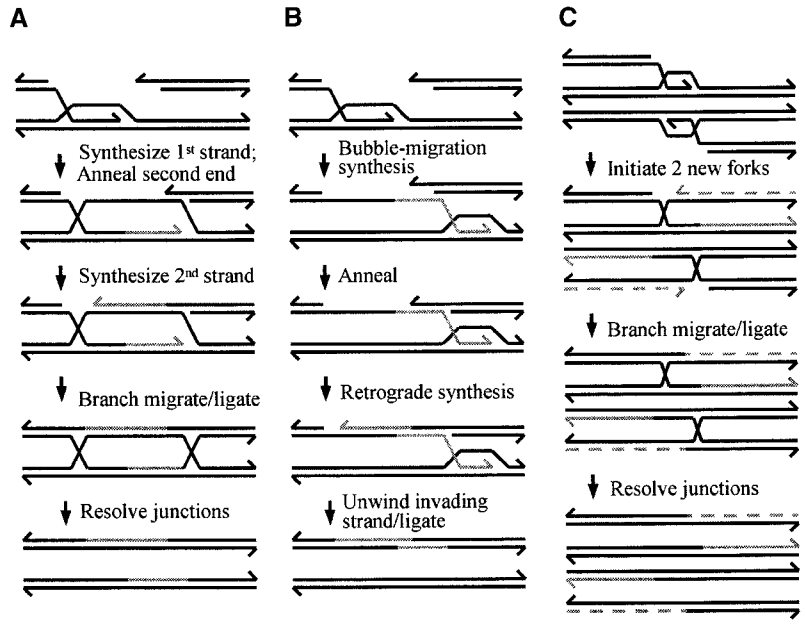

FIGURE 1.—Three models for DSBR during bacteriophage T4 infection: (A) the SZOSTAK *et al.* (1983) model (MUELLER *et al.* 1996a); (B) the synthesis-dependent strand annealing (SDSA) model (MUELLER *et al.* 1996a); and (C) the extensive chromosome replication (ECR) model (GEORGE and KREUZER 1996; GEORGE *et al.* 2001). Each model begins with the initial strand invasion step(s) following processing of the broken ends to generate 3′ single-strand overhangs. Newly synthesized leading- and lagging-strand DNA is denoted by solid and dashed gray lines, respectively. For each model, only one of several possible resolutions is depicted.

than the end of a T4 chromosome. The ECR model is also related to proposed mechanisms for recombinational restart of collapsed replication forks. In those models, the broken arm of a replication fork invades homologous duplex and initiates semiconservative DNA replication (SEIGNEUR *et al.* 1998; GEORGE *et al.* 2001). Finally, the ECR mechanism is also very similar to that proposed for break-induced replication in *Saccharomyces cerevisiae* (MALKOVA *et al.* 1996; MORROW *et al.* 1997).

As mentioned above, previous studies using plasmid-based assays have provided support for the Szostak *et al.*, SDSA, and ECR DSBR models during bacteriophage T4 infection (GEORGE and KREUZER 1996; MUELLER *et al.* 1996a; GEORGE *et al.* 2001). In this article, we present a novel plasmid assay that demonstrates that the two broken ends can undergo repair using two different homologous templates, in support of the ECR model. However, plasmid studies are problematic because the plasmid substrates have limited homology and because rolling-circle replication of the plasmids can distort product recovery. Thus, it remains unclear which of the DSBR mechanisms, if any, predominates *in vivo*, particularly with respect to DSBR involving only phage chromosomal DNA. To address this issue, we have developed a chromosomal DSBR assay to ask whether the two ends of a DSB are repaired in a coordinated fashion as suggested by the Szostak *et al.* and SDSA models or whether the two ends are repaired independently of one another as suggested by the ECR model. As part of this analysis, we have also measured coconversion frequencies during chromosomal DSBR.

MATERIALS AND METHODS

Materials: Restriction enzymes, T4 DNA ligase, and T4 polynucleotide kinase were obtained from New England Biolabs (Beverly, MA), Nytran nylon transfer membranes from Schleicher & Schuell (Keene, NH), random-primed labeling kits from Roche Molecular Biochemicals (Indianapolis), and [α-^{32}P]dATP and [γ-^{32}P]rATP from New England Nuclear (Boston). Oligonucleotides were synthesized by the Duke University Cancer Center DNA Core Facility, and DNA sequencing was performed by the Duke University Cancer Center DNA Analysis Facility. Luria broth (LB) contained Bacto-tryptone (10 g/liter), yeast extract (5 g/liter), and sodium chloride (10 g/liter). Ampicillin and tetracycline were obtained from Sigma (St. Louis) and used at concentrations of 25 μg/ml and 2 μg/ml, respectively, for plasmid-containing strains.

Strains: *Escherichia coli* strains include JGD1 (STOHR and KREUZER 2001), CR63 (*supD*; EDGAR *et al.* 1964), MCS1 λ^+ and MCS1 λ^- (*supD*; both also carry plasmid pKK467, which is irrelevant for these experiments; KREUZER *et al.* 1988), MV20 λ^+ (nonsuppressing; generously provided by Vickers Burdett, Duke University Medical Center, Durham, NC), and NapIV λ^+ (nonsuppressing; NELSON *et al.* 1982) that harbors the *rIIB* expression plasmid pSTS54 (SHINEDLING *et al.* 1986).

Bacteriophage T4 strain K10 carries the following mutations: *amB262* [gene *38*], *amS29* [gene *51*], *nd28* [*denA*], and *rIIPT8* [*denB-rII* deletion] (SELICK *et al.* 1988). T4*td*SG2, which contains a deletion of the I-*Tev*I open reading frame (ORF), was generously provided by Marlene Belfort (State University of New York, Albany, NY; BELL-PEDERSEN *et al.* 1990). John Drake (National Institute of Environmental Health Sciences, Research Triangle Park, NC) kindly provided T4 strains with the following *rII* mutations: AP53, UV232, B94, EM84, FC11, HB84, HB80, HB32, N11, and HB118. All of the mutations are ambers except for FC11 and UV232, both of which are frameshift mutations that have been sequenced previously (SHINEDLING *et al.* 1987; DOAN *et al.* 2001). The *rII* amber mutations were determined by automated sequencing of appropriate PCR fragments from the phage genome. The amber and frameshift *rII* mutations are summarized in Table 1.

Plasmids: Plasmid pBS7 is a pBR322-based plasmid derived from pBS4 (STOHR and KREUZER 2001). One of the two *Ase*I restriction sites of pBS4 was ablated by partial *Ase*I cutting and religation of the vector after filling in the ends with Klenow enzyme, leaving only the *Ase*I site located within the ampicillin resistance gene. The 170-bp *Bgl*II/*Nhe*I fragment containing the T4 replication origin *ori(34)* was then excised and replaced

with a 503-bp, PCR-generated *Bgl*II/*Nhe*I fragment containing 491 bp of pBS4 sequence adjacent to the I-*Tev*I recognition site. The fragment is oriented so that pBS7 contains direct repeats separated by 737 bp of intervening sequence, which includes the I-*Tev*I recognition site. Plasmid pBS8 is identical to pBS7 except that the *Xho*I-flanked, 56-bp I-*Tev*I recognition site has been excised. Plasmid pAC500 was constructed by amplifying a 497-bp fragment of pBS4 sequence adjacent to the I-*Tev*I recognition site using primers containing *Eco*RI restriction sites. The resulting 515-bp *Eco*RI fragment was then inserted into the *Eco*RI site of pACYC184 to generate pAC500. Figure 2A shows schematics of plasmids pBS7 and pAC500.

Plasmid pEC1 was constructed by first cloning an 867-bp *Hin*dIII fragment of the T4 genome containing the *rIIA/B* junction into the *Hin*dIII site of pBR322. An *Xho*I linker with the palindromic sequence 5′-CCTCGAGG-3′ was inserted at the *Ssp*I site near the center of the *rII* fragment. The I-*Tev*I recognition site from pBS4 was excised using *Xho*I and cloned into the *Xho*I linker in the *rII* fragment. The resulting insert at the *Ssp*I site of the *rII* fragment is 64 bp in total length (linker plus I-*Tev*I recognition site).

Construction of new T4 strains: The BAS1 phage strain carrying both the UV232 and the HB80 *rII* mutations was constructed by crossing phage carrying the UV232 and HB80 *rII* single mutations. The double mutant progeny were identified by their inability to grow on MV20 λ^+, MCS1 λ^+, and NapIV λ^+/pSTS54. The two mutations were confirmed by automated sequencing. Phage strain BAS2, which carries the UV232 and HB80 *rII* mutations as well as an I-*Tev*I ORF deletion, was generated by crossing BAS1 with T4*td*SG2 and screening for progeny carrying both *rII* markers (as described above) and the I-*Tev*I ORF deletion (by PCR analysis).

Phage strain BAS3, which carries the I-*Tev*I ORF deletion and an I-*Tev*I recognition site interrupting the beginning of the *rIIB* gene, was generated by marker rescue from plasmid pEC1 using the T4*td*SG2 phage strain. Because the I-*Tev*I site and linker introduce 64 bp into the beginning of the *rIIB* gene, they cause an inactivating frameshift mutation. Phage carrying the I-*Tev*I recognition site in *rIIB* were initially identified by their inability to grow on MV20 λ^+, and the presence of the I-*Tev*I ORF deletion was checked by PCR. Proper integration of the I-*Tev*I recognition site in *rIIB* was confirmed by automated sequencing.

Phage strain HB80-SG2 was generated by crossing the HB80 *rII* mutant with T4*td*SG2 and selecting for progeny carrying the HB80 mutation and the I-*Tev*I ORF deletion.

Plasmid recombination assay: Aliquots of frozen log-phase JGD1 cells harboring plasmids pAC500 and either pBS7 or pBS8 were diluted 1:200 into LB containing ampicillin and tetracycline and grown with shaking at 37° to an OD_{560} of 0.5 ($\sim 4 \times 10^8$ cells/ml). Phage strain K10 was added at a multiplicity of infection (MOI) of 3 and incubated for 4 min at 37° without shaking to allow phage adsorption. Cultures were incubated with vigorous shaking for an additional 36 min, with 1-ml aliquots removed at indicated times. DNA purification, digests, gel electrophoresis, and Southern blotting were performed as described previously (Stohr and Kreuzer 2001).

Coconversion assay: CR63 was grown to an OD_{560} of 0.5 and co-infected with BAS3 at an MOI of 1 and one of the *rII* single mutants at an MOI of 6. After a 4-min adsorption at 37° without shaking, infections were continued for an additional 41 min at 37° with vigorous shaking. Infected cells were then lysed with chloroform at room temperature for 30 min and cell debris was removed by centrifugation (8000 × *g* for 10 min). Total phage titers and rII^+ recombinant phage titers were determined by plating lysate dilutions on MCS1 λ^- and MV20 λ^+, respectively.

Plaque hybridization was used to detect BAS3 phage in which the I-*Tev*I site had not been cut and to detect phage carrying the I-*Tev*I ORF deletion. For both analyses, plaques on MCS1 λ^- plates were transferred to Nytran membranes per manufacturer protocol (Schleicher & Schuell). Oligonucleotide probes specific for either the I-*Tev*I ORF deletion (5′-GTA GAACCCGGGCAGTC-3′) or the *rII* region I-*Tev*I recognition site (5′-CGTTGAGCTCGAGGATTGTA-3′) were kinase labeled with [γ-^{32}P]rATP using T4 polynucleotide kinase. Hybridizations were performed using a modification of the procedure described in Woods *et al.* (1989). Plaque hybridizations were visualized using a PhosphorImager (Molecular Dynamics, Sunnyvale, CA).

Phage recombination assay: CR63 was grown to an OD_{560} of 0.5 and co-infected with BAS3 at an MOI of 0.1 and BAS1 at an MOI of 9. Infections, lysate preparation, and determination of total phage titers and rII^+ recombinant phage titers were as described above for the coconversion assay. Titers of $rIIA^-$ single mutant recombinants were determined by plating on MCS1 λ^+, which supports $rIIA^-$ and rII^+ recombinant growth, and subtracting out the rII^+ recombinant titer. Similarly, $rIIB^-$ recombinant titers were determined by plating on the NapIV λ^+/pSTS54 cell line, which supports $rIIB^-$ and rII^+ recombinant growth, and subtracting out the rII^+ recombinant titer. Determination of $rIIB^-$ single mutant recombinants was complicated by a low efficiency of plating on the NapIV λ^+/pSTS54 cell line. This problem was circumvented by first preadsorbing the phage to CR63 for 4 min and then plating on NapIV λ^+/pSTS54 cells on plates containing 400 μg/ml carbenicillin. Control experiments demonstrated that this procedure raised efficiency of plating of $rIIB^-$ single mutants to 90–100% of that on MCS1 λ^- (data not shown).

RESULTS

Two-plasmid assay to detect ends-apart DSBR: Previous plasmid studies have provided strong evidence for the ECR model of DSBR (George and Kreuzer 1996; George *et al.* 2001). In these studies, however, the plasmids were designed such that both ends of the DSB could potentially utilize the same homologous plasmid molecule as a repair template. We have designed a modified two-plasmid assay that forces the two ends of the DSB to undergo repair using homologous templates on two different plasmid molecules (Figure 2A). Plasmid pBS7 contains a cloned recognition site for the phage-encoded endonuclease I-*Tev*I. An ~500-bp region to the left of the I-*Tev*I site is homologous to plasmid pAC500 (Figure 2A, dark gray boxes) while an ~500-bp region to the right of the I-*Tev*I site has been duplicated in a direct orientation at another location on the pBS7 plasmid (Figure 2A, light gray boxes). The plasmids do not contain cloned T4 origins of replication and will therefore not undergo origin-directed replication during T4 infection (Kreuzer and Alberts 1985).

Following T4 infection, the I-*Tev*I endonuclease should cleave pBS7, thereby stimulating DSBR. If ends-apart repair can occur, the homologous segments of the two plasmids will align as diagrammed in Figure 2B. This repair will generate both an interplasmid recombinant between pBS7 and pAC500 and an intraplasmid recombinant (repeat deletion) within the pBS7 molecule it-

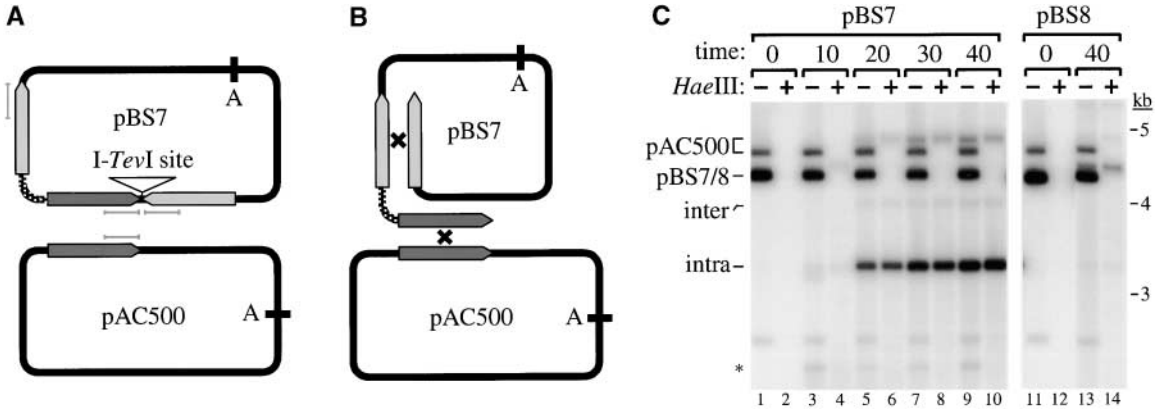

FIGURE 2.—Ends-apart repair of plasmid DSBs. (A) Schematic diagram of the pBS7 and pAC500 plasmids. The I-*Tev*I recognition site has been described previously (GEORGE and KREUZER 1996). Light and dark gray boxes indicate regions of homology. Bars labeled A denote *Ase*I restriction sites. Gray lines indicate probe hybridization sites. The stippled portion of the pBS7 plasmid indicates the region of the plasmid that should not be traversed by DSBR-induced replication forks according to ECR model predictions (see accompanying text for details). (B) Predicted alignment of homologous segments following cleavage at the I-*Tev*I recognition site. (C) Plasmid DSBR time course. *E. coli* harboring the pAC500 plasmid and either the pBS7 (plus I-*Tev*I site) or the pBS8 (minus I-*Tev*I site) plasmid were infected with T4 strain K10. Sample collection times are indicated above each lane (minutes postinfection). The zero time point samples were collected immediately preceding phage addition. DNA was digested with *Ase*I alone (odd-numbered lanes) or *Ase*I plus *Hae*III (even-numbered lanes), and plasmid bands were visualized using a probe for the regions of plasmid homology. The nonrecombinant plasmid bands and the expected interplasmid (inter) and intraplasmid (intra) recombinants are labeled. Note that phage-replicated plasmid bands are resistant to *Hae*III cleavage and migrate slightly slower due to glucosylated hydroxymethylcytosine residues. The asterisk indicates one of the two pBS7 fragments generated by I-*Tev*I cleavage; the shorter of these bands has migrated off the gel. The molecular markers were generated by measuring the migration of *Xba*I fragments of unmodified T4 DNA. The phage-replicated pBS8 band that appears in the control infection (lanes 13 and 14) is uncharacterized, but may result from background levels of plasmid breakage and RDR. It appears similar in intensity to the phage-replicated pAC500 band in lanes 9 and 10 because the pBS8 plasmid receives three probe equivalents while the pAC500 plasmid receives only one probe equivalent.

self. According to the ECR model, each invading DSB end will initiate semiconservative replication. Both the pAC500 plasmid and the pBS7 intraplasmid recombinant should therefore be amplified extensively through DSBR-induced rolling-circle replication. However, the pBS7/pAC500 interplasmid recombinant should not be significantly amplified because the repair-induced replication forks are not predicted to traverse the entire length of this recombinant *Ase*I fragment (see Figure 2, A and B).

Cells harboring the pAC500 plasmid and either pBS7 or pBS8 (a control plasmid lacking the I-*Tev*I recognition site) were infected with T4 strain K10, and aliquots were removed at 10-min intervals. The parental plasmids and two expected recombinants were resolved by *Ase*I digestion and Southern blotting using a probe that hybridizes to 200-bp segments on each side of the cloned I-*Tev*I site and to the corresponding homologous regions (Figure 2A, gray lines). The various parental and recombinant bands hybridize unequally to this probe. The pBS7 parental band receives three probe equivalents, the interplasmid recombinant band two probe equivalents, and the intraplasmid recombinant and parental pAC500 bands one probe equivalent. Phage-replicated plasmid bands can be identified by digesting with *Hae*III in addition to *Ase*I. Because phage-replicated bands contain glucosylated hydroxymethylcytosine residues, they are resistant to *Hae*III cleavage and migrate slightly slower than unreplicated (unmodified) bands (KREUZER *et al.* 1988). Hydroxymethylcytosine residues are incorporated by T4 DNA polymerase during DNA replication, and these modified bases are therefore an excellent marker for DNA that has been replicated by the T4 machinery (REVEL 1983).

As the infection progressed, replicated pAC500 plasmid and the expected interplasmid (inter) and intraplasmid (intra) recombinants accumulated in the pBS7/pAC500 samples but not in the control pBS8/pAC500 samples (Figure 2C). As predicted by the ECR model, the pAC500 plasmid and the intraplasmid recombinant replicated extensively, and the interplasmid recombinant band was extremely weak. The phage-replicated status of the pAC500 plasmid was evident from its slightly slower migration compared to unreplicated plasmid. Furthermore, addition of *Hae*III to the digests had little or no effect on the intensities of both the replicated pAC500 and the intraplasmid recombinant bands, and therefore both were largely or totally replicated by the T4 machinery. Interestingly, the interplasmid recombinant was also largely or totally resistant to *Hae*III digestion, even though DSBR-induced replication forks are not predicted to traverse the entire recombinant *Ase*I fragment (see Figure 2, A and B). This *Hae*III resistance is likely due to replication of the interplasmid recombi-

nant subsequent to the repair event but could potentially result from the repair process itself through an unknown mechanism (George *et al.* 2001).

While both pAC500 and the intraplasmid recombinant replicated extensively, quantitation of the Figure 2C Southern blot indicates that accumulation of the intraplasmid recombinant was ~10-fold greater than accumulation of replicated pAC500. This result suggests that the intraplasmid recombination event is significantly favored over the interplasmid recombination event. This preference is likely due to the fact that interplasmid recombination requires the broken end to encounter a second homologous plasmid, while intraplasmid recombination involves a broken end and repair template tethered together on the same DNA molecule.

These plasmid results strongly suggest that the two ends of a DSB can undergo ends-apart repair while stimulating extensive DNA replication, findings that support the ECR model of DSBR. However, because this assay forces ends-apart repair events, it cannot address whether ends-apart repair predominates *in vivo* when other potential repair mechanisms are possible. In addition, as with all of the other plasmid assays, it is not known whether repair mechanisms demonstrated during plasmid DSBR accurately reflect repair of chromosomal DSBs (see Introduction).

Chromosomal assay to measure coconversion during DSBR: To begin analyzing DSBR mechanisms in the phage genome, we cloned an I-*Tev*I recognition site into the *rIIB* gene of T4. As demonstrated in detail below, when the phage containing the cloned I-*Tev*I recognition site is co-infected with an I-*Tev*I-expressing phage containing flanking *rII* mutations, the I-*Tev*I site is efficiently cleaved. The resulting DSBR reaction leads to a 3.7- to 6.4-fold increase in *rII* recombinant formation (see below), and the system thereby provides a useful tool for analyzing chromosomal DSBR mechanisms.

Using this basic strategy, we first developed an assay to measure coconversion during chromosomal DSBR. While coconversion frequencies have been measured during bacteriophage T4 infection, those studies looked at coconversion during repair events involving phage/plasmid crosses (Bell-Pedersen *et al.* 1989; Mueller *et al.* 1996b; Huang *et al.* 1999). Because the plasmids necessarily shared only limited homology with the T4 genome, the applicability of these results to chromosomal coconversion is unclear.

In our chromosomal coconversion assay, *E. coli* are co-infected with two phage strains as diagrammed in Figure 3A. BAS3 carries an I-*Tev*I recognition site that has been cloned into the beginning of the *rIIB* gene. Because the cloned site is 64 bp in length, it introduces an inactivating frameshift into the *rIIB* gene. BAS3 also has a nearly complete deletion of the I-*Tev*I ORF, allowing propagation of the BAS3 strain without self-cleavage. The co-infecting phage strain carries a single amber or frameshift mutation somewhere within the *rIIA* or *rIIB* genes. Different co-infecting phage with single mutations spanning *rIIA* and *rIIB* are used to measure coconversion frequencies throughout the region. All of the mutations present in the co-infecting strains are ambers, except FC11 and UV232, which are frameshifts resulting from a single base deletion and addition, respectively (Figure 3A; Table 1). The co-infecting phage strains all have an intact I-*Tev*I ORF, so I-*Tev*I endonuclease is expressed during co-infection.

For the coconversion assay infections, BAS3 phage was added at an MOI of 1 and the co-infecting *rII* mutant was added at an MOI of 6. At this input ratio, almost every bacterial cell received multiple copies of the co-infecting *rII* mutant phage, ensuring that almost all of the BAS3 phage were cleaved by I-*Tev*I (see below). In addition, the BAS3 phage was greatly outnumbered by the co-infecting mutant, so that DSBR of cleaved BAS3 almost always occurred using the co-infecting phage as a repair template. Co-infections were terminated after 45 min by the addition of chloroform to lyse the bacterial cells. The total phage titers were determined by plating on the nonselective cell line MCS1 λ^-, while *rII*$^+$ recombinant titers were determined by plating on the lambda lysogen MV20 λ^+, which does not support growth of either parental phage.

As a control, we first asked whether cleavage of the I-*Tev*I recognition site stimulates DSBR and recombination in the *rII* region. For this experiment, we generated a phage carrying both the HB80 *rIIA* mutation and the I-*Tev*I ORF deletion (designated HB80-SG2). We then compared co-infections with BAS3 (at an MOI of 1) and either the original HB80 phage (I-*Tev*I$^+$) or the HB80-SG2 phage (at an MOI of 6). In the latter infection, no I-*Tev*I protein will be made, so the BAS3 I-*Tev*I recognition site will not be cleaved. Formation of the *rII*$^+$ recombinant was ~4.5-fold higher with HB80 than with HB80-SG2 [*rII*$^+$/total pfu = 4.3×10^{-2} ($\pm 0.27 \times 10^{-2}$) and 9.6×10^{-3} ($\pm 0.89 \times 10^{-3}$), respectively]. This experiment demonstrates that a large majority of recombinants result from DSB formation at the I-*Tev*I recognition site.

To generate coconversion curves, BAS3 was co-infected along with the various *rII* mutant phage described above, and the percentage of *rII*$^+$ recombinants in the output phage pool was determined by plating on the selective cell lines. The output percentage of a distant marker, the I-*Tev*I ORF deletion, was also measured by using plaque hybridization (see materials and methods). The I-*Tev*I ORF is ~25 kb from the *rII* region and was therefore not expected to undergo significant coconversion. Indeed, the output percentage of this marker closely matched the input percentage (which is equal to the BAS3 input percentage of 14.3%; data not shown), and therefore the marker is not coconverted at a measurable level.

If all the BAS3 phage are cleaved and use the co-infecting phage as a repair template, the I-*Tev*I site will

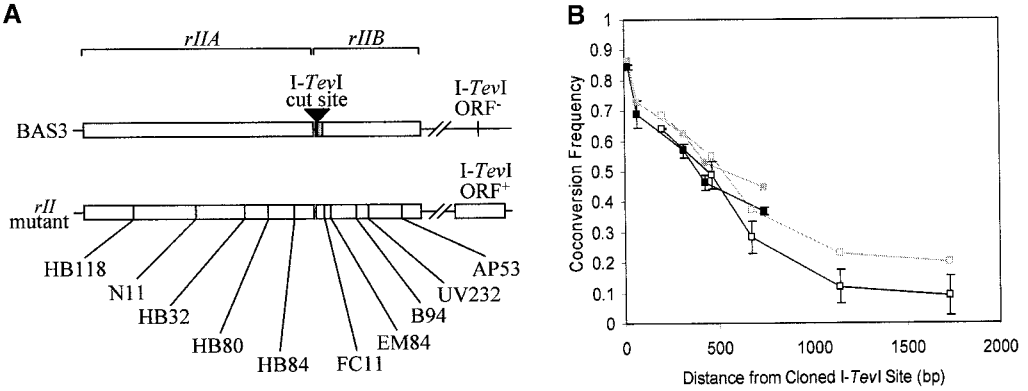

FIGURE 3.—Coconversion of flanking markers during chromosomal DSBR. (A) Phage strains used for coconversion assay. The BAS3 strain contains a cloned I-*Tev*I recognition site (gray box) that causes an inactivating frameshift in the *rIIB* gene and carries a deletion of the I-*Tev*I ORF. The co-infecting *rII* mutant strains each contain one of the 10 *rII* mutations diagrammed and have a wild-type I-*Tev*I ORF. The *rII* region is drawn approximately to scale while the I-*Tev*I ORF region is not. (B) Coconversion curves. The uncorrected and corrected coconversion curves are denoted by the gray and black lines, respectively (see accompanying text for details). The *rIIA* markers are indicated by the open squares (from left to right: HB84, HB80, HB32, N11, and HB118) and the *rIIB* markers are indicated by the solid squares (from left to right: FC11, EM84, B94, UV232, and AP53). The graph shows the mean ± SD from three experiments.

be converted to the corresponding wild-type *rIIB* allele in all cases. These repair events will generate rII^+ phage when coconversion at the flanking site does not occur and *rII* mutant phage when coconversion does occur. Measurement of the rII^+ phage titer following co-infection can therefore be used to calculate coconversion frequency according to the following formula: coconversion = 1 − (rII^+ output percentage/I-*Tev*I ORF deletion output percentage). Figure 3B shows coconversion frequencies throughout the *rII* region generated in this way (gray lines).

We acknowledge that our assay does not allow us to account for all of the products of each individual DSBR event as is possible by tetrad analysis in yeast systems, and our results therefore do not fit the strictest definition of "conversion." However, by analyzing the input and output percentages of alleles surrounding the I-*Tev*I recognition site, we demonstrate reduced recovery of alleles close to the break site, but full recovery of distant alleles (Figure 3B and see below). From this skewed recovery, we can infer that alleles close to the break site have indeed been replaced by the corresponding alleles from the uncut phage genome. We use the terms "conversion" and "coconversion" to refer to this nonreciprocal transfer of *rII* alleles resulting from DSB formation and repair.

TABLE 1

***rII* mutations**

Name	Gene	Base change	Base position	Amber codon position
AP53	*rIIB*	T → C	168,154	250
		G → A	168,156	
UV232	*rIIB*	+T	168,468	NA
B94	*rIIB*	G → A	168,582	108
EM84	*rIIB*	G → A	168,825	27
FC11	*rIIB*	−T	168,875	NA
HB84	*rIIA*	C → T	190	667
HB80	*rIIA*	G → A	452	580
HB32	*rIIA*	C → T	667	508
N11	*rIIA*	G → A	1,136	352
HB118	*rIIA*	G → A	1,724	156

UV232 is an insertion of an extra T in a run of two T's at positions 168,468 and 168,469 of the phage genome (DOAN *et al.* 2001), and FC11 is a deletion of one T from a run of five T's at positions 168,875–168,879 (SHINEDLING *et al.* 1987). All T4 genome coordinates are from the 10/98 release. NA, not applicable.

Several corrections were applied to further refine the coconversion curves. First, control experiments indicated that the efficiency of plating of rII^+ phage on the MV20 λ^+ cell line was only 90% of that on the nonselective cell line MCS1 λ^- (data not shown). This plating deficiency was corrected for by multiplying the calculated rII^+ phage titers by 1.11. Second, control experiments demonstrated that the output percentage of the I-*Tev*I recognition site was ~3% of the input percentage, indicating that a small fraction of the BAS3 input phage were not cleaved at the cloned I-*Tev*I site during the co-infection (data not shown). These uncut phage were identified by plaque hybridization using an oligonucleotide probe specific for the cloned I-*Tev*I site in the *rII* region. These uncut phage effectively lower the BAS3 pool capable of generating rII^+ recombinants, and coconversion frequencies were adjusted accordingly by multiplying the I-*Tev*I ORF deletion output percentage in the coconversion equation above by 0.97. These corrections resulted in a small but significant change in the slopes of the coconversion curves (Figure 3B, black lines).

As anticipated, markers close to the I-*Tev*I cleavage site were frequently coconverted while markers far from the cut site were rarely coconverted. The coconversion curves are quite symmetrical with respect to the I-*Tev*I site, and coconversion frequencies do not appear to be affected by mutation type (amber *vs.* frameshift). We

argue below that the shape of the coconversion curves is primarily due to exonucleolytic degradation and that mismatch repair is unlikely to be a major factor (see DISCUSSION). The coconversion frequencies of HB80 and UV232, both ~0.5, are utilized in the following section to analyze DSBR mechanisms.

Chromosomal assay to analyze coordination of DSB ends during repair: The coconversion assay was modified to address whether the two ends of a DSB are coordinated during repair as suggested by the Szostak *et al.* and SDSA models or whether the two ends of the break are repaired independently as proposed in the ECR model. The modified assay is diagrammed in Figure 4A. Co-infections included BAS3 as before, but the co-infecting phage in this case was BAS1, which carries the two *rII* mutations, HB80 and UV232. These mutations flank the I-*Tev*I site on both sides by ~500 bp and, as demonstrated above, both undergo coconversion ~50% of the time during DSBR.

DSBR of the cleaved BAS3 is expected to generate rII^+, $rIIA^-$, $rIIB^-$, and $rIIA^-B^-$ recombinants. The rII^+, $rIIA^-$, and $rIIB^-$ recombinant titers were determined by plating the phage lysates on the following selective cell lines. MV20 λ^+ is a nonsuppressing lambda lysogen that supports only rII^+ growth. MCS1 λ^+ is a suppressing lambda lysogen that allows growth of rII^+ and $rIIA^-$ recombinants, since HB80 is an amber mutation. Finally, NapIV λ+/pSTS54 supports growth of rII^+ and $rIIB^-$ recombinants by providing the *rIIB* gene product from the pSTS54 plasmid. The efficiency of plating of $rIIB^-$ phage on this strain is low, so the diluted phage lysate is preadsorbed to CR63 before plating (see MATERIALS AND METHODS). Because the $rIIA^-B^-$ recombinants are indistinguishable from the input BAS1 phage, they cannot be enumerated.

As in the coconversion assay, we first sought to analyze the effect of I-*Tev*I cleavage on recombination in the *rII* region during co-infection. For these experiments, we utilized a control phage BAS2 that is identical to BAS1 except that it carries the I-*Tev*I ORF deletion. Therefore, during BAS3/BAS2 co-infections, no I-*Tev*I protein is expressed and the BAS3 I-*Tev*I recognition site is not cleaved. We compared co-infections with BAS3 (at an MOI of 0.1) and either BAS1 or BAS2 (at an MOI of 9). The $rIIA^-$ recombinants were ~3.7-fold higher in the BAS3/BAS1 co-infection than in the BAS3/BAS2 co-infection [$rIIA^-$/total pfu = 3.2×10^{-3} ($\pm 0.31 \times 10^{-3}$) and 8.7×10^{-4} ($\pm 0.025 \times 10^{-4}$), respectively], and the rII^+ recombinants were ~6.4-fold higher [rII^+/total pfu = 6.4×10^{-4} ($\pm 0.94 \times 10^{-4}$) and 1.0×10^{-4} ($\pm 0.061 \times 10^{-4}$), respectively]. These results confirm that the large majority of recombinants observed in the BAS3/BAS1 co-infections are the result of I-*Tev*I site cleavage and subsequent DSBR.

To determine if the ends of a chromosomal DSB are coordinated during the repair process, we performed BAS3/BAS1 co-infections with the BAS3 phage at an MOI of 0.1 and the BAS1 phage at an MOI of 9. The low MOI of BAS3 ensures that almost all of the bacterial cells that are infected by BAS3 will be infected by only a single BAS3 particle, thereby simplifying the calculations described in the APPENDIX and supplementary material at http://www.genetics.org/supplemental/. The high MOI of BAS1 ensures that essentially every bacterial cell is infected by multiple BAS1 particles. As a result, cleaved BAS3 will almost exclusively utilize BAS1 as a template for DSBR, again simplifying the calculations described in the APPENDIX. Furthermore, at this phage input ratio, the three DSBR models make different predictions about the ratios of expected recombinants. Because so many BAS1 repair templates are potentially available to each cleaved BAS3 molecule, the ECR model predicts that the two ends of the DSB will in most instances utilize different BAS1 templates for repair. These ends-apart events can generate $rIIA^-$ and $rIIB^-$ recombinants but not rII^+ recombinants, leading to a relatively high *rII* single mutant to rII^+ recombinant ratio. In contrast, the Szostak *et al.* and SDSA models predict that the two broken ends will always use the same BAS1 template for repair. Such repair will generate both *rII* single mutant and rII^+ recombinants during the repair process, leading to a relatively low *rII* single mutant to rII^+ recombinant ratio.

Using the coconversion frequencies for the HB80 and UV232 *rII* mutations determined above, the predicted *rII* single mutant to rII^+ recombinant ratios were calcu-

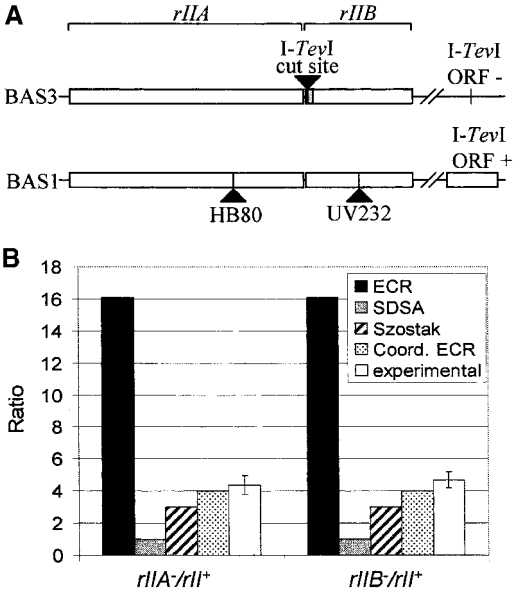

FIGURE 4.—Coordination of ends during chromosomal DSBR. (A) Phage strains used to analyze end coordination. BAS3 is described in the Figure 3 legend. BAS1 carries both the HB80 and UV232 *rII* mutations and a wild-type I-*Tev*I ORF. (B) Predicted and experimental *rII* single mutant to rII^+ recombinant ratios. Predictions for the four DSBR models were calculated as described in the APPENDIX. Experimental values represent the mean ± SD of three experiments.

lated for the three DSBR models and compared to the experimental data (Figure 4B; see DISCUSSION, APPENDIX, and supplementary material at http://www.genetics.org/supplemental/ for description of model prediction calculations and assumptions). The experimentally derived *rII* single mutant to rII^+ ratios of 4.4 and 4.7 (for $rIIA^-$ and $rIIB^-$, respectively) are much closer to the Szostak *et al.* prediction of 3 than to the ECR prediction of ~16, suggesting that the broken ends are largely repaired in a coordinated manner. While the SDSA prediction of 1 does not fit the experimental data as closely as the Szostak *et al.* prediction, adjusting the underlying assumptions used to derive the SDSA prediction can potentially bring it into close agreement with the experimental results (see DISCUSSION and APPENDIX). However, adjusting the underlying assumptions for the ECR model does not bring it into close agreement with the data (see DISCUSSION and APPENDIX). Thus, our data argue that the ECR model, as previously formulated, is not the predominant DSBR pathway *in vivo*. Our results do not distinguish between the other two models.

We next asked whether a variation of the ECR model might fit the experimental data. The ECR model proposes that the two ends of the DSB are free to dissociate and choose different repair templates. However, an ECR model can also be formulated in which the two ends are not free to dissociate. This model, termed coordinated ECR, assumes that the two DSB ends are sequentially repaired, with the second end using a product of the first reaction as repair template (see below and Figure 5). The predicted *rII* single mutant to rII^+ recombinant ratio for the simplest version of the coordinated ECR model is shown in Figure 4B and matches extremely well with the experimentally observed recombinant ratios. Thus, while the original ECR model is largely ruled out by the experimental data, the coordinated ECR model is quite consistent with experimental observation.

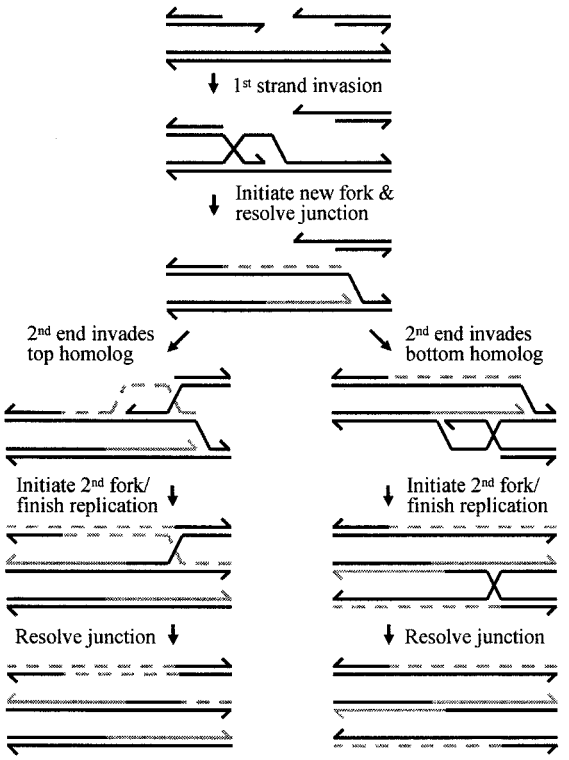

FIGURE 5.—The coordinated ECR model of DSBR. The repair pathway splits on the basis of which homolog the second broken end invades. Newly synthesized leading- and lagging-strand DNA is denoted by solid and dashed gray lines, respectively. Only one of several possible resolutions is depicted.

DISCUSSION

We have asked whether the two ends of a DSB are repaired in a coordinated manner as predicted by the Szostak *et al.* and SDSA models or whether they are repaired independently of one another as predicted by the ECR model. Our plasmid assay results confirm that ends-apart DSBR can occur during T4 infection and that such repair is linked to extensive DNA replication, consistent with ECR model predictions. However, results from the chromosomal DSBR assay indicate that the majority of DSB ends are repaired in a coordinated manner, a finding inconsistent with the ECR model as originally conceived.

As shown in Figure 4B, a modified version of the ECR model fits the experimental results very well. This coordinated ECR model is diagrammed in Figure 5. As with ECR, coordinated ECR begins with one end of the DSB undergoing strand invasion and initiating semiconservative DNA replication. In the case of coordinated ECR, however, the second DSB end is not free to dissociate and utilize another repair template. Instead, it uses one of the two products of the first replication event, initiating a second round of semiconservative DNA replication in the process. The coordinated ECR model is attractive because it explains both the coordination of the DSB ends and the ability of DSBR to initiate extensive DNA replication. As with the original ECR model, the coordinated ECR model fits well with the central role of RDR in the T4 life cycle.

While arguing against uncoordinated ends-apart DSBR as the predominant *in vivo* pathway, our results cannot distinguish between the three coordinated models discussed—Szostak *et al.*, SDSA, and coordinated ECR. The predictions for these models are sensitive to several assumptions that may not be accurate. First, our predictions for Figure 4B assume that coconversion of the HB80 allele and coconversion of the UV232 allele occur in a random and independent manner during each repair event. If this assumption is altered, it could potentially raise or lower the predicted *rII* single mutant to rII^+ recombinant ratios for the coordinated repair models. Second, for the Szostak *et al.* prediction in Figure 4B, we assumed that Holliday junctions are resolved

in a completely random manner, which may not be true. Skewed Holliday junction resolution could potentially alter the predicted Szostak *et al.* recombinant ratio in either direction. Finally, we assumed that coconversion is due strictly to double-strand exonucleolytic resection of the broken ends (see below). If single-strand exonucleolytic resection contributes to the frequency of coconversion, the predicted *rII* single mutant to *rII*$^+$ recombinant ratios for the Szostak *et al.* and SDSA models would be higher (see APPENDIX). Due to uncertainty about these assumptions, we cannot rule out any of the coordinated DSBR models. Furthermore, it is very possible that multiple DSBR mechanisms occur during phage infection, together accounting for the observed recombinant ratios. Because our results cannot distinguish between the various coordinated DSBR models, we have not attempted to calculate recombinant predictions for the many variations of these models that appear in the literature.

The prediction of the original version of the ECR model is sensitive to several of the same assumptions as the coordinated model predictions. Of particular interest are those assumptions that, if altered, could bring the ECR prediction closer to the experimental results. For example, if we assume that double-strand exonucleolytic resection is absolutely symmetrical with respect to each DSB rather than random as assumed for the Figure 4B prediction, the predicted *rII* single mutant to *rII*$^+$ recombinant ratio for the ECR model drops to ~7.5 (calculations not shown). Alternatively, if we assume that coconversion of the HB80 and UV232 markers is due entirely to single-strand exonucleolytic resection rather than to double-strand resection as assumed for the Figure 4B prediction, the predicted *rII* single mutant to *rII*$^+$ recombinant ratio for the ECR model drops to ~8.5 (calculations not shown). While either of these changes brings the ECR model predictions closer to the experimental results, the ECR predictions are still significantly higher than the experimentally determined ratios. Furthermore, we believe that both of these assumptions are very unlikely to be true, at least in their extreme forms. First, MUELLER *et al.* (1996b) found that coconversion tracts resulting from T4 DSBR in a plasmid-phage system are more often asymmetric than symmetric. Second, on the basis of the shape of the coconversion curves, we argue below that double-strand exonucleolytic resection plays a substantial role in the coconversion of the flanking *rII* markers. Thus, while varying certain assumptions may lower the predicted *rII* single mutant to *rII*$^+$ recombinant ratio for the ECR model, we have not found any reasonable set of assumptions that brings the prediction of the original ECR model into good agreement with the experimental results.

An interesting issue raised by these results is the mechanism by which coordination of the two DSB ends is achieved, regardless of the exact repair pathway. While many potential repair templates are available throughout the bacterial cell, a broken chromosome may have access to only one (or a small subset) of these templates. For example, the phage chromosomes could be anchored to cellular components in such a way that the two DSB ends are constrained to a single nearby template. Another possibility is that coordination of the DSB ends is mediated by specific protein interactions. A strong candidate for this role is the gp46/47 protein complex (CROMIE *et al.* 2001). Several recent studies on gp46/47 homologs in eukaryotic systems have suggested that this protein complex may be important for coordinating the ends of a DSB. First, human Rad50/Mre11 can bind to double-strand DNA ends *in vitro*, and interactions between multiple Rad50/Mre11 complexes can tether two DNA ends together (DE JAGER *et al.* 2001). Second, mutations in either the *RAD50* or the *MRE11* genes in *S. cerevisiae* led to aberrant DSBR recombination events, possibly caused by a lack of coordination between the two ends of the break (RATTRAY *et al.* 2001). Finally, the Rad50/Mre11 structure is consistent with a role in linking DNA ends (ANDERSON *et al.* 2001; DE JAGER *et al.* 2001). While the T4 gp46/47 complex is smaller than its eukaryotic counterparts, it contains all of the conserved catalytic and structural domains (SHARPLES and LEACH 1995; CROMIE *et al.* 2001). Thus, gp46/47 might play a role in coordinating repair of DSBs.

The gp46/47 complex might also play an important role in shaping the coconversion curves presented in Figure 3B, as it is believed to be the primary enzyme responsible for processing DSB ends during T4 infection (reviewed in KREUZER 2000). Recent *in vitro* data suggest that gp46/47 has a 5′ to 3′ exonuclease activity that may generate the 3′ single-stranded end needed for strand invasion (BLEUIT *et al.* 2001). Furthermore, *S. cerevisiae* strains lacking the gp47 homolog Mre11 show decreased gene conversion tract lengths in a plasmid gap repair assay (SYMINGTON *et al.* 2000). The T4 proteins RNaseH, DexA, and gp43, all of which have DNA exonuclease activity, have also been implicated in coconversion (HUANG *et al.* 1999).

The shape of our coconversion curves could potentially be influenced by mismatch repair, but probably in only a very subtle manner. Mismatched bases in heteroduplex DNA can be cleaved by the gp49 protein *in vitro*, allowing repair by DNA polymerase and ligase (SOLARO *et al.* 1993). Repair of mismatched bases in T4 has also been supported by *in vivo* work (BERGER and PARDOLL 1976; SHCHERBAKOV *et al.* 1982). However, these *in vivo* studies demonstrated that the extent and strand bias of mismatch repair varies widely depending on the type of mismatch and its sequence context. Thus, mismatch repair cannot easily explain the smooth decline of our coconversion curves and the fact that both the amber and the frameshift mutations fall on the same curve. Furthermore, reported levels of *in vivo* mismatch repair during recombination in T4 appear too low to play

a prominent role in shaping the coconversion curves (markers most prone were repaired only 10% of the time; Shcherbakov *et al.* 1978). Interestingly, the one *rII* amber marker in our study that does not fall directly on the coconversion curves is AP53, the only amber codon resulting from two base substitutions (see Table 1). Perhaps AP53 is more prone to mismatch repair, resulting in a small but significant effect on its coconversion frequency.

Assuming that end resection largely determines the shape of the coconversion curves, what is the nature of this resection? If resection were solely on the 5′ strand, we would expect the highest coconversion frequency to be 0.5, but markers within ~500 bp of the DSB were well above this level. Thus, the data strongly indicate that double-strand exonucleolytic resection makes a major contribution to the shape of the coconversion curves, particularly for the closer markers. However, single-strand 3′ ends are important for each of the DSBR models, implying that resection of the 5′ and 3′ strands does not occur strictly in parallel. We presume that the 5′ strand tends to be resected farther than the 3′ strand, but we currently have no good way of judging this difference.

Previous studies of coconversion during T4 infection looked at flanking markers during intron movement between the phage genome and plasmid substrates (Bell-Pedersen *et al.* 1989; Mueller *et al.* 1996b; Huang *et al.* 1999). Because the plasmids necessarily shared limited homology with the genome, markers far from the DSB site were flanked by only a small amount of homologous sequence, which could potentially reduce their coconversion frequencies. Consistent with this interpretation, our chromosomal assay (with unlimited homology) gives significantly higher coconversion frequencies for distant markers compared to those of previous plasmid/phage studies. For example, the Huang *et al.* (1999) study found that a marker ~500 bp from the I-*Tev*I site was coconverted ~30% of the time, while we find that a marker at that distance is coconverted ~50% of the time.

One of the previous studies also found that *in vivo* coconversion curves are slightly asymmetric with respect to the I-*Tev*I break site (Mueller *et al.* 1996b). *In vitro* analysis suggested that this asymmetry could result from the I-*Tev*I protein remaining bound to one side of the break after cleavage, thereby protecting it from exonuclease degradation (Mueller *et al.* 1996b). In our assay, such protection should lead to lower coconversion frequencies of the *rIIB* markers since the I-*Tev*I binding site is on the *rIIB* side of the break. We see no indication of such bias in our chromosomal system (Figure 3B), indicating that either the I-*Tev*I protein does not bind the broken DNA end *in vivo* or such binding does not significantly affect coconversion frequencies.

Coordination of DNA ends during DSBR is likely critical in eukaryotic systems for maintaining genomic stability. For instance, coordinated DSBR may help to avoid chromosomal duplication resulting from repair of DSBs (Cromie *et al.* 2001). Furthermore, end coordination is likely important in the repair of Spo11-induced breaks during yeast meiosis (Hunter and Kleckner 2001). The mechanisms by which such coordination is achieved in eukaryotic systems remain speculative. In light of the results presented here, phage T4 may serve as a good model system with which to explore the fundamental mechanisms of end coordination during DSBR.

We gratefully acknowledge John Drake for helpful discussion during assay development and for providing numerous *rII* mutant strains. We also thank Vickers Burdett and Marlene Belfort for providing bacterial and phage strains and Dan Tomso for preliminary work on this project. This work was supported by research grant GM-34622 from the National Institutes of Health (NIH). B.A.S. was supported in part by the NIH Medical Scientist Training Program grant T32-GM07171-26.

LITERATURE CITED

Anderson, D. E., K. M. Trujillo, P. Sung and H. P. Erickson, 2001 Structure of the Rad50 × Mre11 DNA repair complex from *Saccharomyces cerevisiae* by electron microscopy. J. Biol. Chem. **276:** 37027–37033.

Belfort, M., 1990 Phage T4 introns: self-splicing and mobility. Annu. Rev. Genet. **24:** 363–385.

Bell-Pedersen, D., S. M. Quirk, M. Aubrey and M. Belfort, 1989 A site-specific endonuclease and co-conversion of flanking exons associated with the mobile *td* intron of phage T4. Gene **82:** 119–126.

Bell-Pedersen, D., S. Quirk, J. Clyman and M. Belfort, 1990 Intron mobility in phage T4 is dependent upon a distinctive class of endonucleases and independent of DNA sequences encoding the intron core: mechanistic and evolutionary implications. Nucleic Acids Res. **18:** 3763–3770.

Berger, H., and D. Pardoll, 1976 Evidence that mismatched bases in heteroduplex T4 bacteriophage are recognized *in vivo*. J. Virol. **20:** 441–445.

Bleuit, J. S., H. Xu, Y. Ma, T. Wang, J. Liu *et al.*, 2001 Mediator proteins orchestrate enzyme-ssDNA assembly during T4 recombination-dependent DNA replication and repair. Proc. Natl. Acad. Sci. USA **98:** 8298–8305.

Cromie, G. A., J. C. Connelly and D. R. Leach, 2001 Recombination at double-strand breaks and DNA ends: conserved mechanisms from phage to humans. Mol. Cell **8:** 1163–1174.

de Jager, M., J. van Noort, D. C. van Gent, C. Dekker, R. Kanaar *et al.*, 2001 Human Rad50/Mre11 is a flexible complex that can tether DNA ends. Mol. Cell **8:** 1129–1135.

Doan, P. L., K. G. Belanger and K. N. Kreuzer, 2001 Two types of recombination hotspots in bacteriophage T4: one requires DNA damage and a replication origin and the other does not. Genetics **157:** 1077–1087.

Edgar, R., G. Denhardt and R. Epstein, 1964 A comparative study of conditional lethal mutants of bacteriophage T4D. Genetics **49:** 635–648.

George, J. W., and K. N. Kreuzer, 1996 Repair of double-strand breaks in bacteriophage T4 by a mechanism that involves extensive DNA replication. Genetics **143:** 1507–1520.

George, J. W., B. A. Stohr, D. J. Tomso and K. N. Kreuzer, 2001 The tight linkage between DNA replication and double-strand break repair in bacteriophage T4. Proc. Natl. Acad. Sci. USA **98:** 8290–8297.

Huang, Y. J., M. M. Parker and M. Belfort, 1999 Role of exonucleolytic degradation in group I intron homing in phage T4. Genetics **153:** 1501–1512.

Hunter, N., and N. Kleckner, 2001 The single-end invasion: an asymmetric intermediate at the double-strand break to double-

Holliday junction transition of meiotic recombination. Cell **106:** 59–70.

Kreuzer, K. N., 2000 Recombination-dependent DNA replication in phage T4. Trends Biochem. Sci. **25:** 165–173.

Kreuzer, K. N., and B. M. Alberts, 1985 A defective phage system reveals bacteriophage T4 replication origins that coincide with recombination hot spots. Proc. Natl. Acad. Sci. USA **82:** 3345–3349.

Kreuzer, K. N., H. W. Engman and W. Y. Yap, 1988 Tertiary initiation of replication in bacteriophage T4. Deletion of the overlapping *uvsY* promoter/replication origin from the phage genome. J. Biol. Chem. **263:** 11348–11357.

Malkova, A., E. L. Ivanov and J. E. Haber, 1996 Double-strand break repair in the absence of *RAD51* in yeast: a possible role for break-induced replication. Proc. Natl. Acad. Sci. USA **93:** 7131–7136.

Morrow, D. M., C. Connelly and P. Hieter, 1997 "Break copy" duplication: a model for chromosome fragment formation in *Saccharomyces cerevisiae*. Genetics **147:** 371–382.

Mosig, G., 1983 Relationship of T4 DNA replication and recombination, pp.120–130 in *Bacteriophage T4*, edited by C. K. Mathews, E. M. Kutter, G. Mosig and P. B. Berget. ASM Press, Washington, DC.

Mueller, J. E., J. Clyman, Y. J. Huang, M. M. Parker and M. Belfort, 1996a Intron mobility in phage T4 occurs in the context of recombination-dependent DNA replication by way of multiple pathways. Genes Dev. **10:** 351–364.

Mueller, J. E., D. Smith and M. Belfort, 1996b Exon coconversion biases accompanying intron homing: battle of the nucleases. Genes Dev. **10:** 2158–2166.

Nassif, N., J. Penney, S. Pal, W. R. Engels and G. B. Gloor, 1994 Efficient copying of nonhomologous sequences from ectopic sites via P-element-induced gap repair. Mol. Cell. Biol. **14:** 1613–1625.

Nelson, M. A., L. Ericson, L. Gold and J. F. Pulitzer, 1982 The isolation and characterization of TabR bacteria: hosts that restrict bacteriophage T4 rII mutants. Mol. Gen. Genet. **188:** 60–68.

Paques, F., and J. E. Haber, 1999 Multiple pathways of recombination induced by double-strand breaks in *Saccharomyces cerevisiae*. Microbiol. Mol. Biol. Rev. **63:** 349–404.

Rattray, A. J., C. B. McGill, B. K. Shafer and J. N. Strathern, 2001 Fidelity of mitotic double-strand-break repair in *Saccharomyces cerevisiae*: a role for *SAE2/COM1*. Genetics **158:** 109–122.

Revel, H. R., 1983 DNA modification: glucosylation, pp.156–165 in *Bacteriophage T4*, edited by C. K. Mathews, E. M. Kutter, G. Mosig and P. B. Berget. ASM Press, Washington, DC.

Seigneur, M., V. Bidnenko, S. D. Ehrlich and B. Michel, 1998 RuvAB acts at arrested replication forks. Cell **95:** 419–430.

Selick, H. E., K. N. Kreuzer and B. M. Alberts, 1988 The bacteriophage T4 insertion/substitution vector system. A method for introducing site-specific mutations into the virus chromosome. J. Biol. Chem. **263:** 11336–11347.

Sharples, G. J., and D. R. Leach, 1995 Structural and functional similarities between the SbcCD proteins of *Escherichia coli* and the RAD50 and MRE11 (RAD32) recombination and repair proteins of yeast. Mol. Microbiol. **17:** 1215–1217.

Shcherbakov, V. P., G. P. Chirkov, L. A. Plugina, E. A. Kudriashova and S. T. Sizova, 1978 Contribution of correction to genetic recombination in T4 phage measured by the effect of map contraction. Genetika **14:** 122–128.

Shcherbakov, V. P., L. A. Plugina, E. A. Kudryashova, O. I. Efremova, S. T. Sizova *et al.*, 1982 Marker-dependent recombination in T4 bacteriophage. I. Outline of the phenomenon and evidence suggesting a mismatch repair mechanism. Genetics **102:** 615–625.

Shinedling, S., L. T. Walker and L. Gold, 1986 Cloning the complete *rIIB* gene of bacteriophage T4 and some observations concerning its middle promoters. J. Virol. **60:** 787–792.

Shinedling, S., B. S. Singer, M. Gayle, D. Pribnow, E. Jarvis *et al.*, 1987 Sequences and studies of bacteriophage T4 *rII* mutants. J. Mol. Biol. **195:** 471–480.

Solaro, P. C., K. Birkenkamp, P. Pfeiffer and B. Kemper, 1993 Endonuclease VII of phage T4 triggers mismatch correction *in vitro*. J. Mol. Biol. **230:** 868–877.

Stohr, B. A., and K. N. Kreuzer, 2001 Repair of topoisomerase-mediated DNA damage in bacteriophage T4. Genetics **158:** 19–28.

Symington, L. S., L. E. Kang and S. Moreau, 2000 Alteration of gene conversion tract length and associated crossing over during plasmid gap repair in nuclease-deficient strains of *Saccharomyces cerevisiae*. Nucleic Acids Res. **28:** 4649–4656.

Szostak, J. W., T. L. Orr-Weaver, R. J. Rothstein and F. W. Stahl, 1983 The double-strand-break repair model for recombination. Cell **33:** 25–35.

Woods, J. P., J. F. Dempsey, T. H. Kawula, D. S. Barritt and J. G. Cannon, 1989 Characterization of the neisserial lipid-modified azurin bearing the H.8 epitope. Mol. Microbiol. **3:** 583–591.

Communicating editor: L. S. Symington

APPENDIX: DSBR MODEL PREDICTIONS

Recombinant ratio predictions for the four DSBR models were derived utilizing the coconversion frequencies of the HB80 and UV232 *rII* mutations determined above (see Figure 3B). The experimentally determined values were 0.49 ± 0.05 for HB80 and 0.46 ± 0.02 for UV232. Since these two values were not significantly different from each other and were very close to 0.5, both coconversion frequencies were rounded to 0.5. As a result, the predictions for the $rIIA^-/rII^+$ and $rIIB^-/rII^+$ recombinant ratios are equivalent for each model.

For the model predictions, we assumed that coconversion of the HB80 and UV232 markers occurs in a random and independent manner during each repair event and that this coconversion results from double-strand exonucleolytic destruction of the corresponding wild-type alleles (see DISCUSSION). However, wild-type allele destruction might sometimes result from single-strand exonucleolytic resection as well. If we assume that single-strand resection makes a significant contribution to coconversion of the HB80 and UV232 markers, the predicted *rII* single mutant to rII^+ recombinant ratios for the Szostak *et al.* and SDSA models would rise, while the predicted ratios for the ECR and coordinated ECR models would fall. However, even if we make the unlikely assumption that HB80 and UV232 coconversion is entirely due to single-strand exonucleolytic resection, the predicted *rII* single mutant to rII^+ recombinant ratio for the ECR model is still significantly higher than the experimentally observed ratios (see DISCUSSION).

To simplify model predictions, end coordination experiments were performed at a BAS3 MOI of 0.1 and a BAS1 MOI of 9. The low BAS3 MOI ensures that almost all of the bacterial cells infected by BAS3 were infected by only a single BAS3 particle. The ~90% of cells not infected by BAS3 are excluded from further analysis since they could not generate any recombinant phage. The high BAS1 MOI ensures that essentially all of the bacterial cells were infected by multiple BAS1 particles. Control experiments demonstrate that our infections fit the Poisson distribution quite closely (data not shown), and so the fraction of bacterial cells receiving different numbers of BAS1 particles can be closely approximated using the Poisson equation. The high BAS1 to BAS3 ratio ensures that, even if several rounds of phage replication occur prior to I-*Tev*I site cleavage and repair, the cleaved BAS3 molecule will almost always

utilize a BAS1 molecule as a repair template rather than another BAS3 molecule or a previously formed recombinant molecule.

Since all of the coordinated models propose that the two ends of the break utilize the same template for repair, the predicted *rII* single mutant to rII^+ recombinant ratio can be calculated by considering the possible outcomes of a single cleaved BAS3 molecule undergoing repair by utilizing a single BAS1 template molecule. In contrast, the ECR model proposes that the two ends may use different templates for repair. Thus, ECR predictions must account for the number of potential repair templates available to the cleaved BAS3 molecule during infection.

Below, we describe the basic approach and additional assumptions used for the model predictions. A more detailed explanation of the calculations is available on the GENETICS website at http://www.genetics.org/supplemental/.

SZOSTAK *et al.* (1983) model: An additional assumption made in deriving the Szostak *et al.* prediction is that Holliday junction resolution is random. This assumption is important only in repair events in which neither *rII* marker is coconverted (which should represent approximately one-quarter of the total repair events). In this case, random junction resolution will generate an rII^+ recombinant 50% of the time and one $rIIA^-$ recombinant and one $rIIB^-$ recombinant 50% of the time. Using this assumption, we predict an *rII* single mutant to rII^+ recombinant ratio of 3 for the Szostak *et al.* model. If we assume instead that Holliday junction resolution is not random, it could have the effect of either raising or lowering the predicted *rII* single mutant to rII^+ recombinant ratio.

SDSA model: The SDSA predictions are very similar to those of the Szostak *et al.* model. The primary difference is that in repair events in which neither *rII* marker is coconverted, Holliday junction resolution is not a factor with SDSA (as we assume an SDSA mechanism in which resolution is by strand unwinding only). Therefore, such repair events will always generate an rII^+ recombinant. As a result, the predicted *rII* single mutant to rII^+ recombinant ratio for the SDSA model is 1, threefold lower than the Szostak *et al.* prediction.

Coordinated ECR model: The coordinated ECR mechanism is diagrammed in Figure 5. For simplicity, we assume that the two ends of the break do not invade the homologous duplex simultaneously and that replication initiated at the first invading end has traversed the *rII* region prior to invasion of the second end of the break. We also assume that the second DNA end has an equal chance of invading either of the homologs generated from the first replication event (see Figure 5). Using these assumptions, the predicted *rII* single mutant to rII^+ recombinant ratio for the coordinated ECR model is 4.

ECR model: We first derived the predicted recombinant frequencies for bacterial cells containing a single BAS3 chromosome and from 1 to 18 BAS1 chromosomes. The predictions vary in each case since the two ends of the cleaved BAS3 molecule have different numbers of template molecules available for repair. The contribution of each of these infected cell types to the recombinant frequencies of the mass lysate was weighted by the probability of a cell containing that number of BAS1 chromosomes (determined using the Poisson distribution). For simplicity, we assumed that the phage burst sizes were constant for bacterial cells containing different numbers of BAS1 chromosomes. While this assumption is probably not strictly true, it will not significantly affect our predictions. If we instead assume that cells infected by fewer BAS1 particles have smaller burst sizes, the predicted *rII* single mutant to rII^+ recombinant ratio for the ECR model will be even higher. Finally, the weighted recombinant frequencies were summed to give the overall recombinant frequencies for the mass lysate, which were then converted to recombinant ratios. The resulting predicted *rII* single mutant to rII^+ recombinant ratio for the ECR model is 16.1.